 SDHM, vol.7, no.3, pp.191-209, 2011

# Crack Growth Simulation in Integrally Stiffened Structures Including Residual Stress Effects from Manufacturing. Part II: Modelling and Experiments Comparison

**S.M.O. Tavares[1], S.M. Häusler[2], P.M. Baiz[3], P.M.S.T. de Castro[1]
P. Horst[2] and M.H. Aliabadi[3]**

**Abstract:** This article is the second part of a two parts paper which presents, compares and discusses the different crack growth simulation models which were introduced for fatigue crack growth assessment during the DaToN project. In the first part, different simulation approaches were applied to determine a calibration of the stress intensity factors as a function of the crack length for a two stiffeners panel with a central crack. Due to the residual stress field promoted by the different manufacturing processes, its influence was included in the numerical models to determine the stress intensity factors. In this second part, the stress intensity factors calibrations are applied in different crack growth models in order to determine the fatigue life under cyclic loads. Paris, Walker, Forman and NASGRO were used for this purpose. The incorporation of the load ratio variation and of the effect of the residual stresses is in general possible in all of them allowing to determine the influence of the residual stress field in the fatigue crack growth.
The results were tested and compared with experimental results with the purpose of validation of the models.
These numerical models demonstrate that (*i*) it is possible to predict the fatigue life in stiffened welded panels and *(ii)* the residual stress field originated by welding processes can be detrimental or beneficial depending on the location where the crack starts.

**Keywords:** stiffened panels, integral structures, fatigue crack growth laws, experimental crack propagation comparison, residual stress.

[1] IDMEC-FEUP, Universidade do Porto, Portugal. (IDMEC)
[2] Technische Universitat Braunschweig, Germany. (IFL)
[3] Imperial College London, UK. (IMPERIAL)

## 1 Introduction

Fatigue cracking is the most common problem in aeronautical structures, requiring a damage tolerant design philosophy in order to increase their reliability. The evaluation of new design and manufacturing concepts for stiffened panels requires an extensive analysis, to understand their behaviour under the presence of a crack.

As mentioned in the first part of this paper, integral designs create continuous paths for the crack growth that have a detrimental effect on the fatigue life of the structure due to the loss of the discontinuity between the skin and stiffeners of frames. The three different manufacturing techniques, applied in the present project – High Speed Machining (HSM), Laser Beam Welding (LBW) and Friction Stir Welding (FSW) were modelled using the classical Fracture Mechanics approach. The stress intensity factor characterising the stress field around the crack tip was calculated taking into account residual stress fields. Afterwards fatigue crack growth laws were used to model the evolution of the crack length as a function of the number of load cycles.

In the first part, different methodologies to evaluate the stress intensity factors were detailed and compared using different approaches of different partners in this project, Hausler (2011). In this second part these solutions will be used in the different crack growth laws, as the Paris or the NASGRO laws.

An important input for the fatigue crack growth laws is the fatigue material properties that can influence the accuracy of the models. These laws are power equations. Due to these facts, an analysis was performed for fitting the experimental data. Several experimental data sets were used to estimate these material parameters for the different fatigue laws.

The influence of the residual stresses in the load ratio at the crack tip is also considered in the fatigue crack growth laws. This load ratio at the crack tip (effective load ratio) is the conjugation of the remote load ratio plus the residual stress field. The Paris law on its own does not consider this load ratio influence in the fatigue behaviour, and that can be a limitation of this law when applied in these types of problems.

The modelled results were compared with the experimental data for the different conditions, with variable accuracy, which indicates that these laws are very sensitive to the inputs that usually are measured experimentally, although these models may give good estimations of the fatigue life in integral stiffened panels and allow a faster optimization for higher performance.

## 2 Fatigue Crack Growth Laws

A number of laws may be used to predict the fatigue behaviour. In this study the stiffened panels were manufactured in aluminium alloys, and therefore linear elastic fracture mechanics assumptions are suitable to model their fatigue crack propagation life.

Several laws were applied by the different DaToN partners to model the fatigue life. Paris law, Paris (1963) is the classic law to determine the crack growth:

$$\frac{da}{dN} = C_P \Delta K^{n_P} \tag{1}$$

where $C_P$ and $n_P$ and the material constants. This law just describes the linear part of the fatigue crack propagation behaviour of the materials (phase II) and the load ratio is not considered. Forman (1967) included the effect of the load ratio (R) influence, and the asymptote associated to the fracture toughness of the material ($K_c$):

$$\frac{da}{dN} = \frac{C_F \Delta K^{n_F}}{(1-R)K_c - \Delta K} \tag{2}$$

where $C_F$ and $n_F$ are material constants. Another fatigue law suitable for fatigue crack growth in the phase II, is the Walker law, Walker (1970). This law introduces a exponent m$_W$ in order to improve the accuracy of the growth rate dependence with the load ratio:

$$\frac{da}{dN} = \frac{C_W \Delta K^{n_W}}{(1-R)^{m_W}} \tag{3}$$

A more comprehensive crack growth equation, including the fatigue threshold and fatigue toughness effects and with a better fit for different load ratios is the NASGRO law, NASGRO (2002):

$$\frac{da}{dN} = C_N \left[\left(\frac{1-f}{1-R_{eff}}\right)\Delta K\right]^{n_N} \frac{\left(1-\frac{\Delta K_{th}}{\Delta K}\right)^p}{\left(1-\frac{K_{\max}}{K_C}\right)^q} \tag{4}$$

where $C_N$, $n_N$, p and q are empirically derived constants for the material, $f$ is the crack opening function for plasticity-induced crack closure that has been defined as:

$$f = \begin{cases} \max\left(R, A_0 + A_1 R + A_2 R^2 + A_3 R^3\right) & R \geq 0 \\ A_0 + A_1 R & -2 \leq R < 0 \end{cases} \tag{5}$$

$A$ coefficients are defined as:

$$A_0 = \left(0.825 - 0.34\alpha + 0.05\alpha^2\right) \times \times \left[\cos\left(\frac{\pi}{2}\frac{S_{\max}}{\sigma_0}\right)\right]^{1/\alpha} \tag{6}$$

$$A_1 = (0.415 - 0.071\alpha)\frac{S_{\max}}{\sigma_0} \tag{7}$$

$$A_2 = 1 - A_0 - A_1 - A_3 \tag{8}$$

$$A_3 = 2A_0 + A_1 - 1 \tag{9}$$

where $\alpha$ is a plane stress/strain constraint factor, and $S_{max}/\sigma_0$ is the ratio of the maximum applied stress to the flow stress. NASGRO provides a library with these values for different types of materials, heat treatments and thickness.

The fracture toughness values usually presented at the material databases are for the condition of plane strain fracture. However in thin plates the plane stress condition is predominant and for this condition the fracture toughness depends of the thickness. The next equation can be used to estimate the fracture toughness for thin plate from the value of fracture toughness:

$$\frac{K_c}{K_{Ic}} = 1 + B_k e^{-\left(A_k \frac{t}{t_0}\right)^2} \tag{10}$$

and

$$t_0 = 2.5\left(\frac{K_{Ic}}{\sigma_{ys}}\right)^2 \tag{11}$$

where $t$ is the thickness of the plate, the constants $A_k$ and $B_k$ are presented in NASGRO database and $\sigma_{ys}$ is the yield strength of the material.

The threshold stress intensity factor range - $\Delta K_{th}$ - can be approximated by the following expressions:

$$\Delta K_{th} = \frac{\Delta K_1^* \left[\frac{1-R}{1-f(R)}\right]^{\left(1+R\cdot C_{th}^p\right)}}{(1-A_0)^{\left(1-R\cdot C_{th}^p\right)}},\ R \geq 0 \tag{12}$$

and

$$\Delta K_{th} = \frac{\Delta K_1^* \left[\frac{1-R}{1-f(R)}\right]^{\left(1+R\cdot C_{th}^m\right)}}{(1-A_0)^{\left(C_{th}^p-R\cdot C_{th}^m\right)}},\ R < 0 \tag{13}$$

where $\Delta K_1^*$ is calculated by:

$$\Delta K_1^* = \Delta K_1 \left[ \frac{a}{a+a_0} \right]^{1/2} \tag{14}$$

where $\Delta K_1$ is the threshold stress intensity factor range as R $\rightarrow$1.0, $C_{th}$ is an empirical fit constant with different values for positive (superscript p) and negative (superscript m) R ratios, and $a_0$ is a small crack parameter (typical value of 0.0015 inch or $\sim$0.04 mm).

### *2.1 Parameters for the crack growth laws*

The use of representative material data is one of the most important parts of a fatigue crack growth analysis. The tested panels in this project were produced in two different materials: AA6056 and AA2024. The heat treatment is an additional variable to determine the fatigue crack growth constants, however the final heat treatment for the panels in AA6056 was T6 and in AA2024 was T3. Although, when the post-welding heat treatment was not applied, as in the panels "LBW AA6056-T6 as welded", it was not possible to define the real heat condition in the weld region; however this only changes the crack growth condition at the welding line.

#### *2.1.1 AA6056-T6 Fatigue Crack Growth Constants*

Figure 1 shows all the experimental data collected for 6056 aluminium alloy from project partners in DaToN using standardised coupons that were machined from the DaToN panels. A comparison of the FCG behaviour of the plates machined from a block of 40 mm (used for HSM panels) and the plates used in the LBW and FSW panels is shown in this figure.

Paris, Forman and Walker Laws are used because good fits to the experimental data can be obtained with very little effort. As pointed out by Broek (1989), no fatigue crack growth law (Walker, Forman, etc) is fundamentally better than any other, none is more universally useful than any other.

Each set of experimental data could be fitted separately using a power law with their coefficients $C_P$ and $n_P$ being the parameters of the Paris law, as shown by Moreira (2007). Unfortunately, the best fits to the experimental data not always give the best predictions, Broek (1989). The reason for this is that in all curve fitting procedures the same weight is given to each point in the experimental data, while it is known that points at low da/dN levels have a greater influence in the total fatigue life (most of the specimen life is spent during that period). The lack of physical meaning provided by mathematical procedures should be balanced with engineering judgement in order to obtain a representative fit to the real problem.

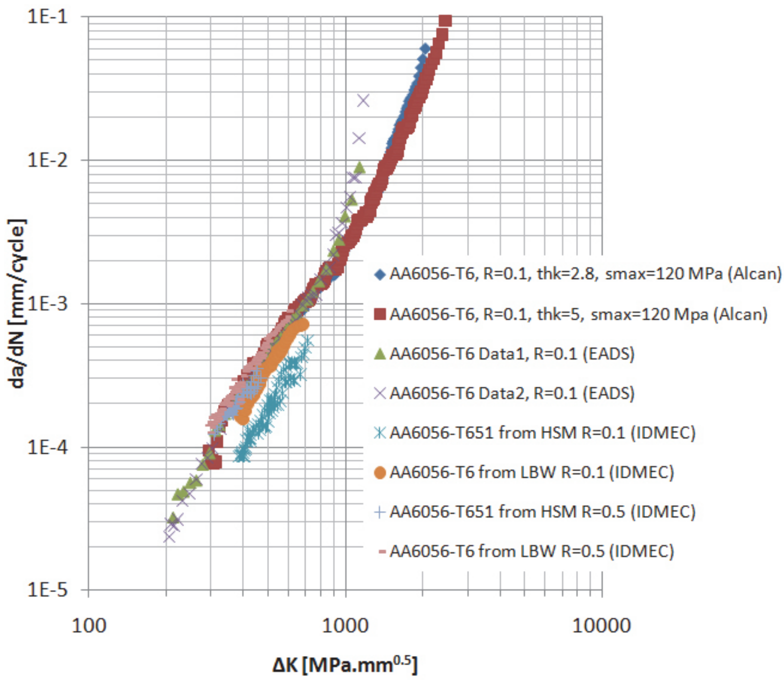


Figure 1: Experimental points for da/dN vs ΔK of AA6056.

Paris Law parameters were set by trying to fit all the experimental data available for each loading ratio. For the loading case of R=0.5, the only 2 sets of data available agree well between them and therefore it is easy to set their values. For the loading case of R=0.1, the scatter is larger and the final fit was set mainly between the experimental data provided by IDMEC, Moreira (2007).

For Forman law several fits were used by the partners in order to determine the best parameters aggregation in order to have a reasonable description for both load ratios (R=0.1 and R=0.5).

An example procedure used to determine the Forman constants was done linearizing the logarithmic values from experimental measurements for both load ratios:

$$\log\left(\frac{da}{dN}\cdot\left[(1-R)\,K_c-\Delta K\right]\right) == n_F \log\left(\Delta K\right)+\log\left(C_F\right) \tag{15}$$

After the value $n_F$ is determined using the least mean squares technique and the $C_F$ value using the minimisation of the error between the Forman law and the experimental points.

Table 1: Fatigue Crack Growth Parameters for AA6056.

| | AA6056-T6 LT | | | |
|---|---|---|---|---|
| | **C** | **n** | **m** | **$K_c$** |
| **Paris R=0.1 (P2)** | 5.00E-12 | 2.850 | -- | -- |
| **Paris R=0.5 (P1)** | 1.00E-11 | 2.850 | -- | .. |
| **Walker (W1)** | 4.42E-12 | 2.850 | 1.179 | |
| **Forman IDMEC (F2)** | 2.90E-07 | 2.351 | -- | 3000 |
| **Forman IFL (F3)** | 4.85E-08 | 2.610 | -- | 3200 |

A variety of different crack growth parameter sets were evaluated that give reasonable approximations of available experimental data.

Paris law parameters obtained for each loading ratio are presented in Table 1. Walker parameters are also given in Table 1 and were obtained from Paris values and using the logarithmic form of equation (3) as shown in Broek (1989). The parameters for the Forman law used are presented in Table 1.

In Figure 2 are presented the fits obtained and are compared with the experimental results for the load ratio R=0.1. Figure 3 shows the same comparison for the load ratio R=0.5.

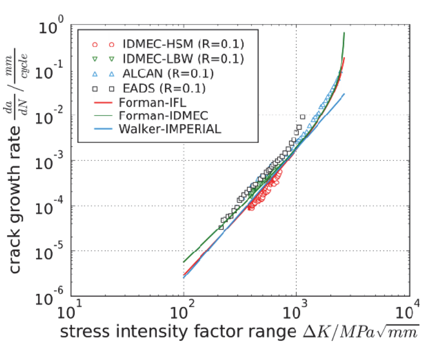


Figure 2: Experimental and empirical crack growth rates for AA6056, R=0.1

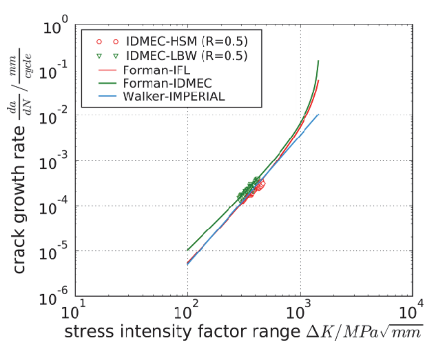


Figure 3: Experimental and empirical crack growth rates for AA6056, R=0.5

### 2.1.2 AA2024-T3 Fatigue Crack Growth Constants

Parameters for 2024-T3 are obtained from the Nasgro software NASGRO (2002). To this material were applied the Forman and NASGRO laws. The Forman parameters were empirically determined from the experimental data presented in the database. The Forman fits were presented in Figure 4 for the load ratio R=0.1 and the values obtained are presented in Table 2.

Table 2: Fatigue Crack Growth Parameters for AA2024-T3.

| | **AA2024-T3 LT** | | |
|---|---|---|---|
| | **C** | **n** | **$K_c$** |
| **Forman 2 IFL (F2)** | 1.65E-08 | 2.780 | 2952 |
| **Forman 3 IFL (F3)** | 2.48E-09 | 3.111 | 2952 |
| **NASGRO (N1)** | 2.38E-12 | 3.20 | 2571 |

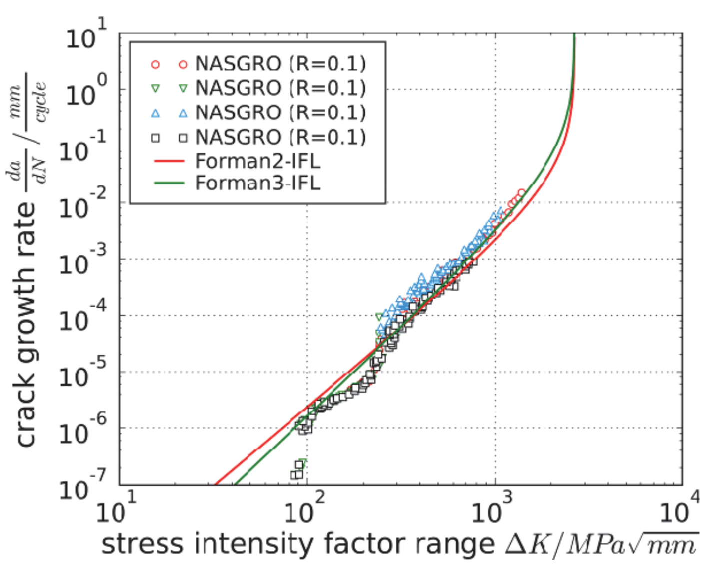


Figure 4: Experimental and empirical crack growth rates for Al-2024 R=0.1

### 2.2 Incorporation of residual stress effects into models

In order to account for the effect of residual stress on fatigue crack growth of metallic structures, several equations have being proposed [Broek (1989), Sadananda (1997), Terada (2005)]. In this project were adopted three of the most known laws, Forman, Walker and NASGRO.

#### 2.2.1 Typical superposition of stress intensity factor (Typical R effective)

The typical approach used for incorporation of residual stresses on fatigue crack growth is based in obtaining an effective stress ratio ($R_{eff}$) that takes into account the residual stress field. This approach can be described in detail by considering the specific cases of Walker or Forman equations, Broek (1989), for example the Forman law to take consideration of a residual stress field can be written as:

$$\frac{da}{dN} = \frac{C_F \Delta K_{eff}^{n_F}}{(1 - R_{eff})K_c - \Delta K_{eff}} \tag{16}$$

where $R_{eff}$ is the effective stress ratio which can be expressed as follows:

$$R_{eff} = \frac{K_{\min} + K_{res}}{K_{\max} + K_{res}} \tag{17}$$

where: $K_{res}$ is the stress intensity factor due to the residual stress field. $\Delta K_{eff}$ is basically $\Delta K$ without residual stress as can be demonstrated by:

$$\Delta K_{eff} = K_{\max_{eff}} - K_{\min_{eff}} = (K_{\max} + K_{res}) - (K_{\min} + K_{res}) = K_{\max} - K_{\min} = \Delta K \tag{18}$$

Thus the effective stress ratio is the only term that considers the effect of residual stress. For this reason, Paris law cannot be used for such purposes, but at the same time any fatigue crack growth law that includes R could be used using the effective load ratio at the crack tip.

Figure 5 shows an example of the evolution of the effective load ratio, calculated from the stress intensity factors of the numerical models with residual stresses, in this case for LBW panels in AA2024-T3 and for the load ratio, R=0.1.

Glinka (1987) introduced an approach which especially accounts for the case of a negative $K_{min,eff}$ due to a large compressive residual stress at low stress ratios $R$. Instead of using a negative $K_{min,eff}$ the approach states that:

$$K_{\min eff} = 0 \text{ for } K_{\min eff} = K_{\min} + K_{res} \tag{19}$$

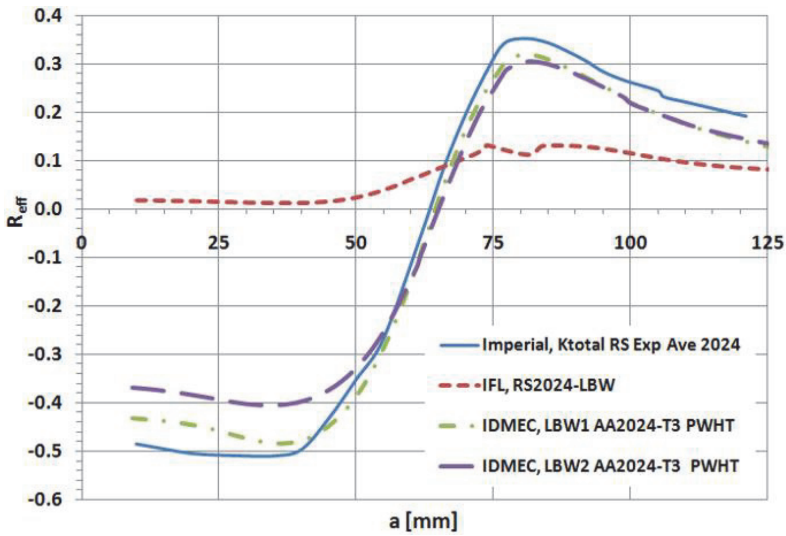


Figure 5: $R_{eff}$ considering the RS of LBW panels in AA2024-T3 and R=0.1.

which is comparable to the investigations on plasticity induced crack closure by Elber (1971). Using $K_{min,eff}$ from Eq. (19) to determine $R_{eff}$ and $\Delta K_{eff}$ so that the following two cases can be differentiated for the superposition approach for usage in the crack growth equations in Eqs. (2) and (3):

- for $K_{min,eff} = K_{min} + K_{res} > 0$:
  the expressions in Eq. (17) and Eq.(18) have to be used for determination of $R_{eff}$ and $\Delta K_{eff}$
- for $K_{min,eff} = K_{min} + K_{res} \leq 0$:
  Eq. (19) leads to the following adapted expressions:

$$\Delta K_{res} = K_{\max} + K_{res} \tag{20}$$

$$R_{eff} = \frac{0}{K_{\max} + K_{res}} = 0 \tag{21}$$

## 3 Modelling

With the stress intensity factors solutions presented in part I and with the integration of the crack growth laws presented above, the fatigue life of the DaToN panels were modelled. For this purpose several algorithms that integrate the fatigue crack growth laws considering the variation of ΔK(a) and the function of $R_{eff}$ were created.

Figure 6 shows the results obtained for the DaToN panels manufactured by High Speed Machining (HSM) in AA6056-T6xx. In the models for HSM panels the residual stress fields due to the manufacturing process are not considered since it does not generate heat and the plasticization during the process is not substantial, therefore the residual stress field is negligible. In these results three different laws were used, Paris, Walker and Forman with the parameters presented in the Table 1 and using the stress intensity factors calculated by each partner.

Figure 7 shows the modelling results for the DaToN panels produced by Laser Beam Welding in AA6056-T6, tested with the load ratio R=0.5 ($\sigma_{max}$=110 MPa), obtained considering the residual stress field promoted the LBW process. In the case of the contribution of Imperial College, the LBW residual stress field was obtained by modelling whereas for the other partners it was measured directly from the panels.

## 4 Experimental results

An extensive experimental program with the DaToN panels was performed by different partners in this project. The procedures and results of this program are detailed described in Lanciotti (2011). Figures 8 and 9 show a summary of these results.

In Figure 8, a plot with the experimental results for panels in AA6056-T6 and tested with the load ratio R=0.1, are presented. It is perceptible that the manufacturing processes change significantly the fatigue life, in this case the HSM gave the lower fatigue life while the LBW with the configuration 2 gives the higher fatigue life. Figure 9 displays the results for the DaToN panels in AA2024-T3 and tested with the load ratio R=0.5. The highest fatigue life in this panel was obtained with the FSW process and the other panels have a similar fatigue life.

## 5 Results comparison and discussion

The comparison between the experimental results and numerical models of the fatigue life for these stiffened panels was done for all manufacturing processes, HSM, LBW and FSW, for the two materials, AA6056-T6 and AA2024-T3 and for the two stress levels corresponding the load ratios R=0.1 and R=0.5. Figures 10 to 27 compile all these results. The panels produced by HSM in Figures 10 to 13. Good convergence in the results was obtained for the panels in AA6056-T6. Although for the panels in AA2024-T3, Figures 12 and 13, some divergence was found. This divergence can be caused by the fatigue constants, which in this case were obtained

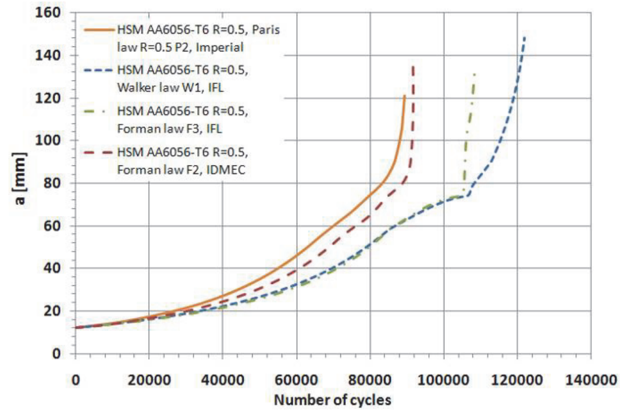


Figure 6: Numerical results of crack growth laws, HSM panels in AA6056-T6, load ratio R=0.1.

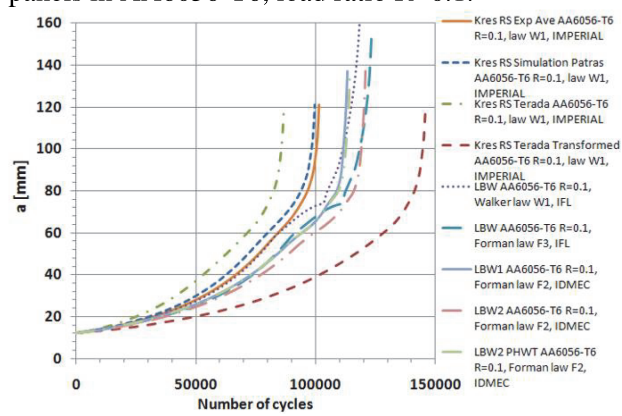


Figure 7: Numerical results of crack growth laws, LBW panels in AA6056-T6, load ratio R=0.5.

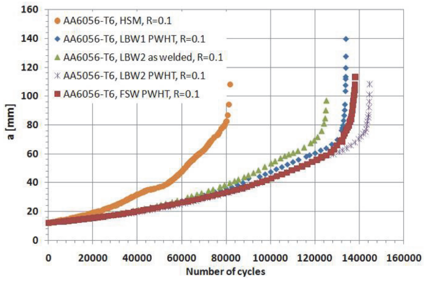


Figure 8: Experimental results from A6056-T6 panels tested at the load ratio R=0.1 ($\sigma_{max}$=80 MPa).

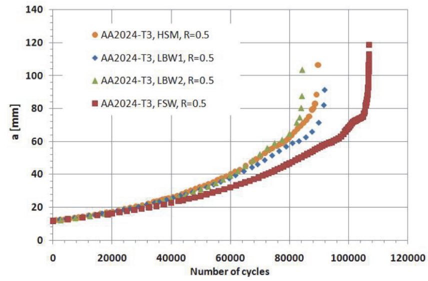


Figure 9: Experimental results from A2024-T3 panels tested at the load ratio R=0.5 ($\sigma_{max}$=110 MPa).

from the NASGRO database and not measured from the material used to produce the panels. Despite the fact that is the same alloy, the properties can be slightly different. In addition, the integration of the fatigue crack growth laws is very sensitive to the material parameters, due to be power laws.

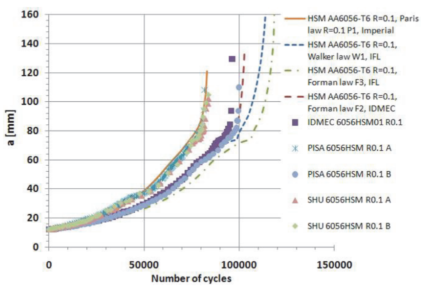


Figure 10: Results comparison, HSM panels in AA6056-T6, load ratio R=0.1.

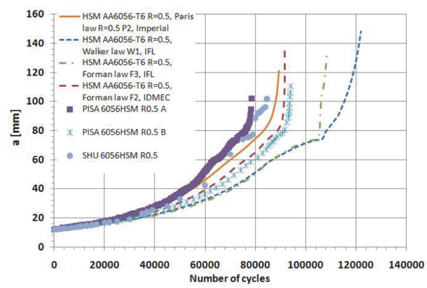


Figure 11: esults comparison, HSM panels in AA6056-T6, load ratio R=0.5.

Figures 14 to 23 exhibit the results comparison for the DaToN panels with stiffeners welded by laser beam. In these panels the residual stress field was incorporated in the models (in the stress intensity factor calculation and in the effective load ratio at the crack tip). Reasonable results of the fatigue life for the most of cases compared with the experimental values were obtained. Although, divergences were found for the panels in AA2024-T3. The reasons for these divergences could be the material parameters, was explained for the HSM panels. One other reason that can increase the divergence is the negative effective load ratios, which instigate some difficulties due crack closure effects in the crack propagation.

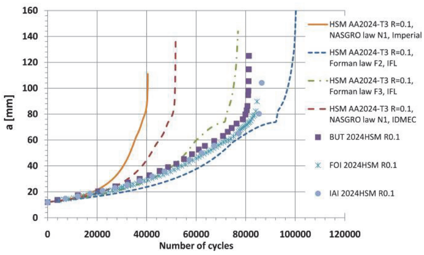


Figure 12: Results comparison, HSM panels in AA2024-T3, load ratio R=0.1.

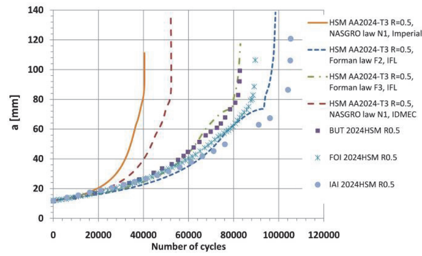


Figure 13: Results comparison, HSM panels in AA2024-T3, load ratio R=0.5.

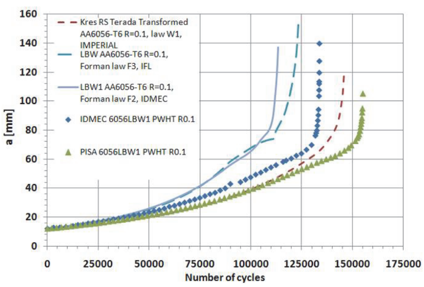


Figure 14: Results comparison, LBW panels in configuration 1, AA6056-T6, load ratio R=0.1.

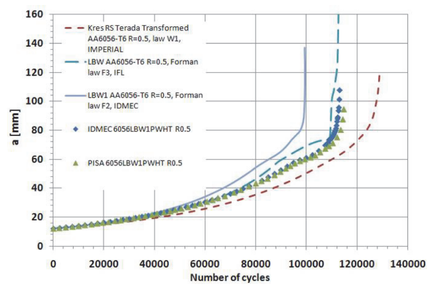


Figure 15: Results comparison, LBW panels in configuration 1, AA6056-T6, load ratio R=0.5.

Negative load ratios were determined when the panels were tested with the remote load ratio of R=0.1. The effect of the crack closure effect is a retardation of the crack growth increasing the fatigue life of the panels, however also in this case, were used the parameters presented in the NASGRO database that can be slightly different of the parameters that describes the material used in the panels.

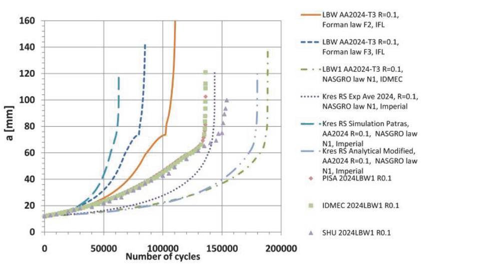


Figure 16: Results comparison, LBW panels in configuration 1, AA2024-T3, load ratio R=0.1.

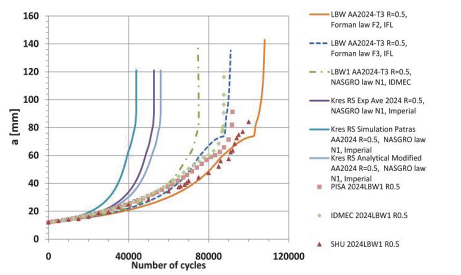


Figure 17: Results comparison, LBW panels in configuration 1, AA2024-T3, load ratio R=0.5.

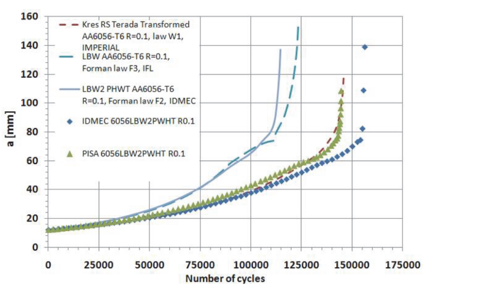


Figure 18: Results comparison, LBW panels in configuration 2 with PWHT, AA6056-T6, load ratio R=0.1.

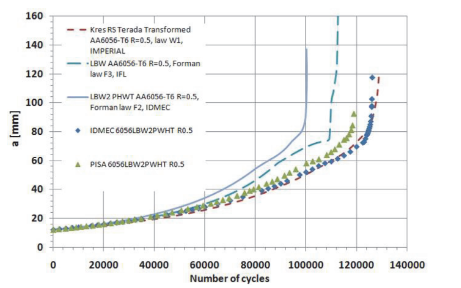


Figure 19: Results comparison, LBW panels in configuration 2 with PWHT, AA6056-T6, load ratio R=0.5.

FSW results comparisons are presented in Figures 24 to 27. As the previous results, in this case also good results were obtained for the panels in AA6056-T6. However for the panels in AA2024-T3 disagreements between the models and the experimental results were found due to the aspects mentioned above, the material base characterization and the negative $R_{eff}$ in the lower crack lengths. For the panels tested at the load ratio R=0.1, this difference is more emphasized due the crack closure effect.

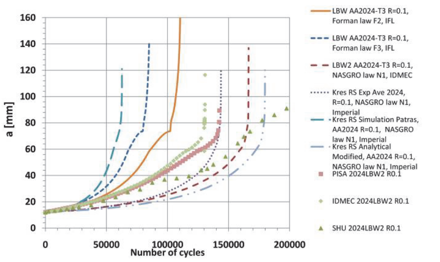


Figure 20: Results comparison, LBW panels in configuration 2 with PWHT, AA2024-T3, load ratio R=0.1.

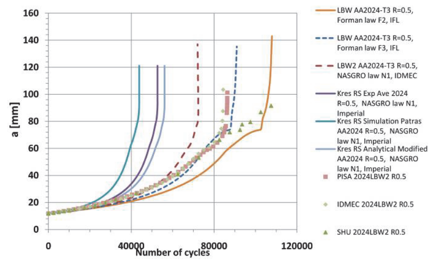


Figure 21: Results comparison, LBW panels in configuration 2 with PWHT, AA2024-T3, load ratio R=0.5.

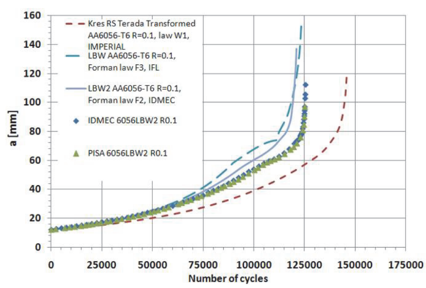


Figure 22: Results comparison, LBW panels in configuration 2 tested as welded, AA6056-T6, load ratio R=0.1.

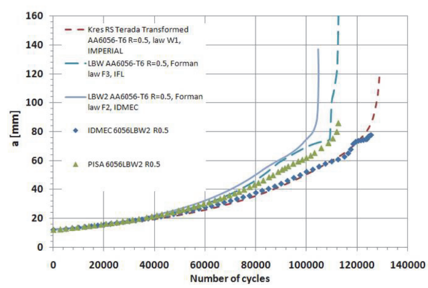


Figure 23: Results comparison, LBW panels in configuration 2 tested as welded, AA6056-T6, load ratio R=0.5.

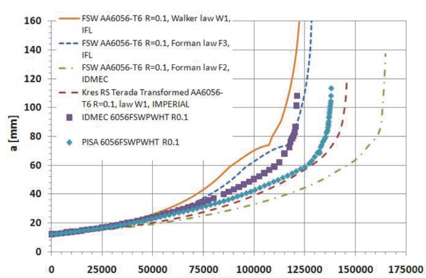


Figure 24: Results comparison, FSW panels in AA6056-T6, load ratio R=0.1.

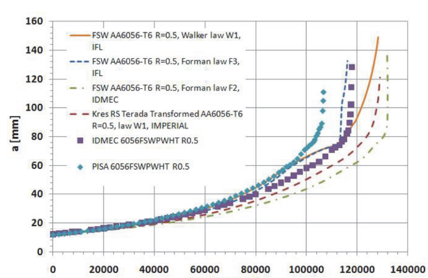


Figure 25: Results comparison, FSW panels in AA6056-T6, load ratio R=0.5.

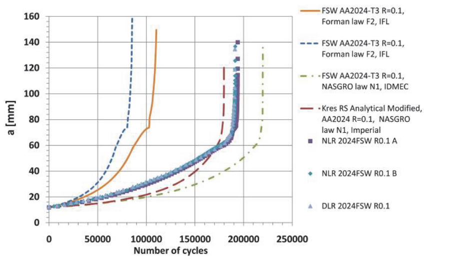


Figure 26: Results comparison, FSW panels in AA2024-T3, load ratio R=0.1.

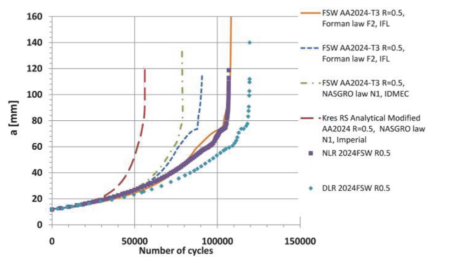


Figure 27: Results comparison, FSW panels in AA2024-T3, load ratio R=0.5.

## 6 Concluding remarks

The models presented in part I and above show the complexity of the different approaches to determine the fatigue life considering the different effects.

A better or worse agreement model *vs.* experiment was associated to the calibration of the stress intensity factors, the models and measurements of the residual stress fields, the material parameters and the fatigue laws.

On the determination of the stress intensity factors, the differences between the different techniques are relatively low, with a good agreement for most of the partners, before the crack reach the stiffeners. The greater part of fatigue life of these panels happens before the crack starts to propagate in the stiffeners.

The incorporation of the residual stress field in the models was not accomplished without difficulty. For example, experimental residual stress field estimation was based on surface measurements with strain gages, and the information along the thickness of the panel was interpolated. The numerical models of residual stress determination require material properties that change with the temperature and strain rates that are not easily determined.

The fatigue material parameters for the fatigue crack growth laws have a large effect on the integration results of these laws. Therefore a correct evaluation of the material parameters is an important aspect in order to obtain reasonable fatigue life estimations.

## 7 Summary and conclusions

Fatigue crack growth models in order to include effects of manufacturing processes are presented in this paper. The most important effect of welding process effect in the fatigue life is the residual stresses originated by the heat input during the process.

The effect of residual stresses can be incorporated in the fatigue crack growth (FCG) estimations by different methods (all of them based on LEFM). FCG in welded structures was obtained using the typical superposition of stress intensity factors in the models and the $R_{eff}$ - effective stress ratio, and a recent approach proposed by Terada, where the effect of residual stresses is accounted as a correction factor to the conventional stress intensity factor range ($\Delta K$). Terada's approach although providing better estimates of fatigue life in some cases, is not always reliable.

Positive results are obtained when advantage is taken of good residual stress estimations with good material parameters estimation. The application of the crack growth parameters from databases could be tricky due to the differences between the different lots of material. Therefore it is recommended to measure these properties from material of the same lot of the material applied in the structure. In addition the negative load ratios promoted by the residual stresses and the crack closure effect require a better interpretation in order to include this effect with higher accuracy in the numerical models.

**Acknowledgement:** The numerical techniques and results presented within this article were developed and acquired during the project DaToN which was funded by the European Commission within the 6th Framework Program. The required materials were generously provided by ALCAN.

## References

**Broek, D.** (1989): *The Practical use of Fracture Mechanics*. Kluwer Academic Publishers, The Netherlands.

**Elber, W.** (1971) The significance of fatigue crack closure. In: Damage tolerance in aircraft structures, ASTM STP 486. Philadelphia (PA): American Society for Testing and Materials, pp. 230–242.

**Forman, R. G.; Kearney, V. E.; Engle, R. M.** (1967): Numerical analysis of crack propagation in cyclic loaded structures. *Transactions of ASME, Journal of Basic Engineering*, vol. 89, pp.459-464.

**Hausler, S.M.; Baiz, P.; Tavares, S.M.O.; Brot, A.; Horst, P.; Aliabadi, F.; de Castro, P.M.S.T.; Peleg-Wolfin, Y.** (2011): Crack growth simulation in integrally stiffened structures including residual stress effects from manufacturing. Part I: model overview, *Structural Durability & Health Monitoring*, vol. , pp. –.

**Lanciotti, A.; Lazzeri, L.; Polese, C.; Rodopoulos, C.; Moreira, P.M.G.P.; Brot, A.; Wang, G.; Velterop, L.; Biallas, G. and Klement, J.** (2011): Fatigue crack growth in stiffened panels, integrally machined or welded (LBW or FSW):

the DaToN project common testing program, *Structural Durability & Health Monitoring*, vol. , pp. -.

**Moreira, P. M. G. P.; Richter-Trummer, V.; Tavares, S. M. O.; de Oliveira, F. M. F.; de Castro, P. M. S. T.** (2007): Characterization of fatigue crack growth rate of AA6056 T651 and T6, Application to DaToN panels life prediction. DaToN–WD5-WP2-WP3–1.0/IDMEC, University of Porto.

**NASGRO** (2002): NASGRO v4.02, Fracture Mechanics and Fatigue Crack Growth Analysis Software.

**Paris, P.; Erdogan F.** (1963): A critical analysis of crack propagation laws. *Trans ASME, Series D*, vol. 85, no. 528.

**Sadananda, K.; Vasudevan, A.K.** (1997): Short Crack Growth and Internal Stresses, *International Journal of Fatigue*, vol. 19, pp. 99-108.

**Terada, H.** (2005): Stress Intensity Factor Analysis and Fatigue Behaviour of a Crack in the Residual Stress Field of Welding. *Journal of ASTM International*, vol. 2, no. 5.

**Walker, K.** (1970): The Effect of Stress Ratio During Crack Propagation and Fatigue for 2024-T3 and 7075-T6 Aluminum, *Effects of Environment and Complex Load History on Fatigue Life, ASTM STP 462*, Rosenfeld, MS, USA.